International Journal of Solids and Structures 47 (2010) 2905–2917

Contents lists available at ScienceDirect

International Journal of Solids and Structures

journal homepage: www.elsevier.com/locate/ijsolstr

Evaluation of self-consistent polycrystal plasticity models for magnesium alloy AZ31B sheet

H. Wang [a], B. Raeisinia [b], P.D. Wu [a,*], S.R. Agnew [b], C.N. Tomé [c]

[a] Department of Mechanical Engineering, McMaster University Hamilton, Ontario, Canada L8S 4L7
[b] Department of Materials Science and Engineering, University of Virginia Charlottesville, VA 22904-4745, USA
[c] Materials Science and Technology Division, Los Alamos National Laboratory, Los Alamos, NM 87545, USA

ARTICLE INFO

Article history:
Received 10 March 2010
Received in revised form 10 June 2010
Available online 25 June 2010

Keywords:
Anisotropic
Constitutive laws
Crystals
Homogenization
Viscoplastic

ABSTRACT

Various self-consistent polycrystal plasticity models for hexagonal close packed (HCP) polycrystals are evaluated by studying the deformation behavior of magnesium alloy AZ31B sheet under different uniaxial strain paths. In all employed polycrystal plasticity models both slip and twinning contribute to plastic deformation. The material parameters for the various models are fitted to experimental uniaxial tension and compression along the rolling direction (RD) and then used to predict uniaxial tension and compression along the traverse direction (TD) and uniaxial compression in the normal direction (ND). An assessment of the predictive capability of the polycrystal plasticity models is made based on comparisons of the predicted and experimental stress responses and *R* values. It is found that, among the models examined, the self-consistent models with grain interaction stiffness halfway between those of the limiting Secant (stiff) and Tangent (compliant) approximations give the best results. Among the available options, the Affine self-consistent scheme results in the best overall performance. Furthermore, it is demonstrated that the *R* values under uniaxial tension and compression within the sheet plane show a strong dependence on imposed strain. This suggests that developing anisotropic yield functions using measured *R* values must account for the strain dependence.

© 2010 Elsevier Ltd. All rights reserved.

1. Introduction

Constitutive modeling of the plastic deformation of Hexagonal Close Packed (HCP) crystals is much more complicated than that in most Face Centered Cubic (FCC) and Body Centered Cubic (BCC) crystals. More specifically, plastic deformation in most FCC and BCC materials is dominated by crystallographic slip, while both slip and twinning contribute to plastic deformation in HCP crystals. Furthermore, due to its low symmetry of crystallographic structure, different types of slip systems exist in an HCP crystal although very few slip systems could be activated at room temperature. At the polycrystal level, an additional difficulty in constitutive modeling for HCP polycrystals is that one must carefully take into account the details of the interaction between crystals/grains, because the effects of these details are more significant than in FCC and BCC materials due to low crystallographic symmetry and high anisotropy in the mechanical behavior of individual grains.

Various polycrystal plasticity models have been developed for polycrystals. Among them, the classic Taylor model (Taylor, 1938) has been the most used, for historic reasons and because of its easy implementation. The Taylor model assumes that all grains must accommodate the same plastic strain equal to the macroscopically imposed strain. This implies that the Taylor model neglects strain variations from grain to grain in the polycrystalline aggregate. As a consequence, the Taylor model does not consider the interaction between crystals, which is believed to be less significant in FCC and BCC materials due to their high crystallographic symmetries. The Taylor model has played an important role in the field of modeling of forming of aluminum and steel sheets (see e.g. Wu et al., 1997; Dawson et al., 2003; Eyckens et al., 2009; Lévesque et al., 2010). For metals like HCP polycrystals with low crystallographic symmetry, stress and strain variations from grain to grain and interaction among grains in a polycrystalline aggregate are significant and cannot be neglected in an attempt to accurately describe deformation behavior. Consequently, polycrystal plasticity models based on the self-consistent approach originally proposed by Kröner (1958), for the elastic case, and later extended to the elastoplastic (Hill, 1965) and viscoplastic (Hutchinson, 1976), are becoming more popular than the Taylor model when modeling HCP polycrystals. In general, self-consistent models allow for different strain response in each grain, depending on the relative stiffness between the grain and a surrounding homogeneous equivalent medium (HEM). The consistency conditions require that the averaged behavior over all the grains must be the same as the

* Corresponding author. Tel.: +1 (905) 525 9140x20092; fax: +1 (905) 572 7944.
E-mail address: peidong@mcmaster.ca (P.D. Wu).

0020-7683/$ - see front matter © 2010 Elsevier Ltd. All rights reserved.
doi:10.1016/j.ijsolstr.2010.06.016

macroscopically imposed one. Among various self-consistent plasticity models, the Visco-Plastic Self-Consistent (VPSC) model developed by Molinari et al. (1987) and extended by Lebensohn and Tomé (1993, 1994) to account for anisotropy, has been widely used to simulate large strain behavior and texture evolution of HCP polycrystalline Mg under various deformation modes (see e.g., Agnew and Duygulu, 2005; Jain and Agnew, 2007; Neil and Agnew, 2009; Proust et al., 2009; Signorelli et al., 2009). Recently, Wang et al. (2010) have developed a finite strain Elastic–Viscoplastic Self-Consistent (EVPSC) model for polycrystalline materials. The EVPSC model is a completely general elastic–viscoplastic, fully anisotropic, self-consistent polycrystal model, applicable at large strain and to any crystal symmetry. However, it has been found that numerical results are extremely sensitive to the stiffness of the grain–matrix interaction associated with the various Self-Consistent Schemes (SCSs) (see e.g. Wang et al., 2010). Therefore, it is necessary to carry out an assessment of the predictive capability of the VPSC/EVPSC model with various SCSs including Secant, Affine, Tangent and the effective interaction m^{eff}.

It is worth mentioning that various SCSs have been evaluated by comparing their predictions, in terms of mechanical responses and texture evolutions, with finite element calculations, full field simulations or available experimental evidence for polycrystals (e.g., Molinari and Tóth, 1994; Tomé, 1999; Lebensohn et al., 2007). It has been found that Secant and Tangent SCSs, among the first-order SCSs, exhibit asymptotic trend to respectively the upper-bound and lower-bound in the rate-insensitive limit, and thus are not appropriate for highly anisotropic materials like HCP polycrystals. The intermediate SCSs, Affine and m^{eff} give better overall predictions, if appropriate artificial parameter m^{eff} is assigned according to results of finite element calculations (e.g., Molinari and Tóth, 1994) or relative directional compliance approach (Tomé, 1999). It has to be noted that those evaluations were based on the assumption that all the material parameters at single crystal level are the same for various SCSs. A real challenge in modeling HCP polycrystals is that it is almost impossible to directly measure the single crystal properties. It has been generally accepted that the differences in stress experienced by differently orientated single crystals in an HCP polycrystal are mainly due to the orientation of a single crystal and the interaction of the single crystal with its surrounding grains. The interaction is, of course, dependent on the self-consistent scheme employed. Therefore, for a textured HCP polycrystal, the only practical way to determine the single crystal properties in a polycrystal plasticity model is by curve-fitting numerical simulations based on the polycrystal model to the corresponding macroscopic experimental data (see Xu et al., 2008). The predicative capability of the polycrystal plasticity model is then assessed by comparing its predictions based on the fitted material constants to the corresponding experiment data other than those used in the fitting. To the best of our knowledge, an assessment for the VPSC and EVPSC models with various SCSs has not been systematically carried out for Mg alloys. However, it is clear that such an assessment is meaningful only if the number of experiments employed is large enough to cover various different deformation processes for a given material. Here, we use for such matter the Mg alloy AZ31B in sheet form, thoroughly characterized experimentally by Jain and Agnew (2007).

In the present study, various self-consistent polycrystal plasticity models for HCP polycrystals are evaluated by studying large strain behavior of magnesium alloy AZ31B sheet under different deformation processes. In all the polycrystal plasticity models employed, both slip and twinning are assumed to contribute to plastic deformations. Values of the material parameters for the various models are fitted to experimental uniaxial tension and compression along the rolling direction (RD) and then used to predict uniaxial tension and compression along the traverse direction (TD) and uniaxial compression in the normal direction (ND). An assessment of the predictive capability of the polycrystal plasticity models is made based on comparisons of the predicted and experimental stress responses and R values. Differences between the predictions of different models are emphasized. For the polycrystal plasticity model with the so-called effective interaction "m^{eff}" scheme, a broader set of parameters is obtained by best fitting to the experimental stress–strain curves and R values under slip-dominated cases of uniaxial tension along the RD and TD and uniaxial compression along the ND. This final exercise permits illustration of the continuum of results which are possible and, notably, span the space between the secant and tangent approximations.

2. Polycrystal plasticity models

Wang et al. (2010) have shown that the differences in the predicted stress–strain curves and texture evolutions based on the EVPSC and the VPSC models are negligible at large strains for monotonic loadings. For deformations involving unloading and strain path changes, the EVPSC predicts a continuous elasto-plastic transition, while the VPSC model gives a discontinuous response due to the lack of elastic deformation. It has been also demonstrated that the EVPSC model can capture some important experimental features associated with elasto-plastic transitions, stress relaxation, and unload, which cannot be simulated with the VPSC model (Wang et al., 2010). Since the deformations studied in the present paper do not involve unloading or strain path changes, our assessment of the predictive capability of the VPSC model with various SCSs also applies to the EVPSC model with the corresponding SCS. For simplicity, the polycrystal SCSs described in what follows refer to the VPSC case.

Plastic deformation of a crystal is assumed to be due to the crystallographic slip and twinning on slip and twinning systems ($\boldsymbol{s}^\alpha$,$\boldsymbol{n}^\alpha$). Here, $\boldsymbol{s}^\alpha$ and $\boldsymbol{n}^\alpha$ are, respectively, the slip/twinning direction and normal direction of the slip/twinning system α in the present configuration. The following equation gives the grain (crystal) level plastic strain rate $\boldsymbol{d}^g$ (see e.g. Asaro and Needleman, 1985):

$$\boldsymbol{d}^g = \sum_\alpha \dot{\gamma}^\alpha \boldsymbol{P}^\alpha, \tag{1}$$

where $\dot{\gamma}^\alpha$ is the shear rate of slip (twinning) system α, and $\boldsymbol{P}^\alpha$ is the associated Schmid tensor:

$$\boldsymbol{P}^\alpha = \frac{1}{2}(\boldsymbol{s}^\alpha \boldsymbol{n}^\alpha + \boldsymbol{n}^\alpha \boldsymbol{s}^\alpha). \tag{2}$$

For slip,

$$\dot{\gamma}^\alpha = \dot{\gamma}_0 \left|\frac{\tau^\alpha}{\tau^\alpha_{cr}}\right|^{\frac{1}{m}} \mathrm{sgn}(\tau^\alpha) \tag{3}$$

and for twinning,

$$\dot{\gamma}^\alpha = \begin{cases} \dot{\gamma}_0 \left(\frac{\tau^\alpha}{\tau^\alpha_{cr}}\right)^{\frac{1}{m}} & \text{for } \tau^\alpha > 0 \\ 0 & \text{for } \tau^\alpha \leqslant 0, \end{cases} \tag{4}$$

where $\dot{\gamma}_0$ is a reference value of slip/twinning rate, m is the slip/twinning rate sensitivity, and τ^α is the resolved shear stress:

$$\tau^\alpha = \boldsymbol{\sigma}^g : \boldsymbol{P}^\alpha \tag{5}$$

τ^α_{cr} is the critical resolved shear stress (CRSS), sgn is the sign function. The evolution of τ^α_{cr} is taken in the form of

$$\dot{\tau}^\alpha_{cr} = \frac{\mathrm{d}\hat{\tau}^\alpha}{\mathrm{d}\gamma_{ac}} \sum_\beta h^{\alpha\beta} \dot{\gamma}^\beta, \tag{6}$$

where $\gamma_{ac} = \sum_\alpha |\gamma^\alpha|$ is the accumulated shear strain in the grain, $h^{\alpha\beta}$ is the latent hardening coupling coefficient which empirically accounts for the obstacles on system α associated with system β. $\hat{\tau}^\alpha$ is the threshold stress and is characterized by

$$\hat{\tau}^\alpha = \tau_0^\alpha + (\tau_1^\alpha + h_1^\alpha \gamma_{ac}) \left(1 - \exp\left(-\frac{h_0^\alpha}{\tau_1^\alpha}\gamma_{ac}\right)\right). \tag{7}$$

Here, τ_0, h_0, h_1 and $\tau_0 + \tau_1$ are the initial CRSS, the initial hardening rate, the asymptotic hardening rate and the back-extrapolated CRSS, respectively. More complex hardening laws have been proposed for Zr by Beyerlein and Tomé (2008) and Proust et al. (2009). These laws regard grains as composite inclusions consisting of parent grain and twin bands and are not considered here. The main purpose of this paper is to analyze the grain–matrix interaction effects on mechanical response of HCP polycrystals rather than the role played by the hardening law.

Various homogenization methods have been developed to characterize the mechanical behavior of a polycrystalline aggregate from the responses of their single crystals. Among them, the most popular Taylor model assumes that the strains of each grain are equal to the imposed macroscopic strains, and the macroscopic stresses are the average of the stresses over all the grains. Another popular homogenizing method is the self-consistent approach, which assumes each grain as an ellipsoidal inclusion embedded in a homogeneous effective medium (HEM), which is the aggregate of the grains. The Eshelby inclusion formalism (Eshelby, 1957), modified for incompressible media by Lebensohn et al. (1998) is used to describe the interaction between each grain and the aggregate. During each deformation step, the single crystal constitutive rule, which describes the grain-level response, and the self-consistency criteria are solved simultaneously. This enables the grain-level stresses and strain rates to be consistent with the boundary conditions imposed on the surrounding polycrystalline aggregate.

To apply the inclusion formalism, in connection with the non-linear visco-plastic response, it is first necessary to linearize the response. For a comprehensive discussion and comparison of the different linearization procedures the reader is referred to Lebensohn et al. (2007). In this Section we only report the relevant equations and in the following Sections we concentrate on discussing the predictions of the different approaches for Mg AZ31, by comparison with available experimental information. The linearized behavior of an inclusion (single crystal) can be written as

$$\boldsymbol{d}^g = \boldsymbol{M}^g : \boldsymbol{\sigma}^g + \boldsymbol{d}_0^g, \tag{8}$$

where $\boldsymbol{M}^g$ and $\boldsymbol{d}_0^g$ are the visco-plastic compliance and the back-extrapolated term of grain g, respectively. The linearized behavior of the HEM (polycrystal) is analogous to the inclusion and is written as

$$\boldsymbol{D} = \overline{\boldsymbol{M}} : \boldsymbol{\Sigma} + \boldsymbol{D}_0, \tag{9}$$

where $\overline{\boldsymbol{M}}, \boldsymbol{D}, \boldsymbol{\Sigma}$ and $\boldsymbol{D}_0$ are the visco-plastic compliance, strain rate, stress and the back-extrapolated term of the HEM, respectively.

Different SCSs depend on different choices for the linearization. Among various SCSs, the Secant SCS employs the following linearization:

$$\begin{aligned} M_{ijkl}^{g,secant} &= \dot{\gamma}_0 \sum_\alpha \left(\frac{\tau^\alpha}{\tau_{cr}^\alpha}\right)^{\frac{1}{m}-1} \frac{P_{ij}^\alpha P_{kl}^\alpha}{\tau_{cr}^\alpha}, \\ d_{0ij}^{g,secant} &= 0, \end{aligned} \tag{10}$$

while the Affine SCS applies the linearization:

$$\begin{aligned} M_{ijkl}^{g,\mathrm{Affine}} &= \frac{\dot{\gamma}_0}{m} \sum_\alpha \left(\frac{\tau^\alpha}{\tau_{cr}^\alpha}\right)^{\frac{1}{m}-1} \frac{P_{ij}^\alpha P_{kl}^\alpha}{\tau_{cr}^\alpha}, \\ d_{0ij}^{g,\mathrm{Affine}} &= \left(1 - \frac{1}{m}\right) d_{ij}^g. \end{aligned} \tag{11}$$

The relation of grain-level stress and strain rate to the aggregate response is obtained self-consistently by

$$(\boldsymbol{d}^g - \boldsymbol{D}) = -\widetilde{\boldsymbol{M}} : (\boldsymbol{\sigma}^g - \boldsymbol{\Sigma}) \tag{12a}$$

with the interaction tensor $\widetilde{\boldsymbol{M}}$ being given by

$$\widetilde{\boldsymbol{M}} = (\boldsymbol{I} - \boldsymbol{S})^{-1} : \boldsymbol{S} : \overline{\boldsymbol{M}}, \tag{12b}$$

where $\boldsymbol{S}$ is the Eshelby tensor for a given grain, $\boldsymbol{I}$ is the identity tensor. The condition that $\boldsymbol{D} = \langle \boldsymbol{d}^g \rangle$ and $\boldsymbol{\Sigma} = \langle \boldsymbol{\sigma}^g \rangle$ (where $\langle \cdots \rangle$ denotes the volume average), leads to a self-consistent equation giving the macroscopic compliance as:

$$\overline{\boldsymbol{M}} = \langle \boldsymbol{M}^g : \boldsymbol{B}^g \rangle : \langle \boldsymbol{B}^g \rangle^{-1} \tag{13a}$$

with

$$\boldsymbol{B}^g = (\boldsymbol{M}^g + \widetilde{\boldsymbol{M}}) : (\overline{\boldsymbol{M}} + \widetilde{\boldsymbol{M}})^{-1}. \tag{13b}$$

As can be seen in Eq. (12b), the interaction tensor $\widetilde{\boldsymbol{M}}$ is approximately proportional to the macroscopic visco-plastic compliance $\overline{\boldsymbol{M}}$, which is itself given by a weighted average of the visco-plastic compliances, $\boldsymbol{M}^g$, of grains (Eq. (13a)). As a consequence, a larger visco-plastic compliance for Affine SCS leads to a larger interaction tensor $\widetilde{\boldsymbol{M}}$ and, as Eq. (12) indicates, will have associated a higher strain heterogeneity compared to Secant SCS. Clearly, since the macroscopic compliance is a weighted average of the single grain compliances, it will be of the same order of magnitude. An example of this is the relation: $\overline{\boldsymbol{M}}^{\mathrm{Tangent}} = \overline{\boldsymbol{M}}^{\mathrm{secant}}/m$ (Hutchinson, 1976). As a consequence, the interaction tensor in the Tangent self-consistent scheme is given by:

$$\widetilde{\boldsymbol{M}} = \frac{1}{m}(\boldsymbol{I} - \boldsymbol{S})^{-1} : \boldsymbol{S} : \overline{\boldsymbol{M}}^{\mathrm{secant}}. \tag{14}$$

Based on the upper and lower limits represented by the Secant and Tangent approaches, Molinari and Tóth (1994) and Tomé (1999) explore using an empirical adjustable parameter m^{eff}, such that $m < m^{eff} < 1$. The m^{eff} scheme provides an intermediate interaction tensor:

$$\widetilde{\boldsymbol{M}} = \frac{1}{m^{eff}}(\boldsymbol{I} - \boldsymbol{S})^{-1} : \boldsymbol{S} : \overline{\boldsymbol{M}}^{\mathrm{secant}}. \tag{15}$$

For details concerning the self-consistent equations associated with the different visco-plastic self-consistent algorithms, we refer the interested reader to Lebensohn et al. (2007).

The Predominant Twin Reorientation (PTR) scheme proposed by Tomé et al. (1991) is used in the present paper to model the reorientation by twinning. Within each grain g, the PTR scheme tracks the shear strain $\gamma^{\alpha,g}$ contributed by each twinning system α, and the associated volume fraction $V^{\alpha,g} = \gamma^{\alpha,g}/\gamma^{tw}$ as well. Here γ^{tw} is the characteristic shear (constant) associated with twinning. Crystallographically equivalent twins belong to the same twin mode. For example, the {10.2} twinning systems which are activated by c-axis tension constitute the tensile twin mode. The sum over all twin systems associated with a given twin mode, and then over all the grains, represents the 'accumulated twin fraction' $V^{acc,mode}$ in the aggregate for the particular twin mode:

$$V^{acc,mode} = \sum_g \sum_\alpha V^{\alpha,g}. \tag{16}$$

In the PTR scheme developed by Tomé et al. (1991), after each deformation increment, a grain is randomly selected to check if the predominant twinning system exceeds a threshold value. If so, the grain is entirely reoriented to a new orientation according to predominant twinning system. The volume fraction of this reoriented grain is added to the so called 'effective twin fraction', $V^{eff,mode}$. The process is repeated until either all grains are checked or the effective twin fraction exceeds the accumulated twin frac-

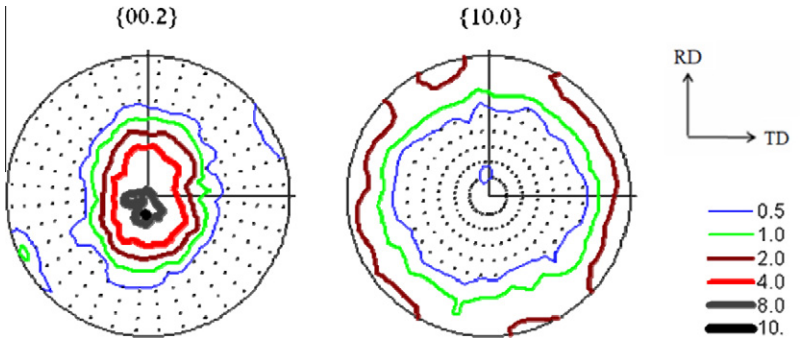

Fig. 1. Initial texture of AZ31B sheet represented in terms of the {00.2} pole figure (a) and {10.0} pole figure (b).

tion. In the latter case, the reorientation by twinning is ceased and the next deformation step is considered. The aforementioned threshold value is defined as

$$V^{th,mode} = A^{th1} + A^{th2}\frac{V^{eff,mode}}{V^{acc,mode}}, \tag{17}$$

where A^{th1} and A^{th2} are two material constants. This approach statistically solves the practical problem that the number of orientations would grow continually if each activated twinning system was represented by a new orientation. Additionally, it maintains the twinned volume fraction at a level that is consistent with the shear activity of the twins contributing to the deformation.

For simplicity, VPSC models with Affine, Secant, Tangent and m^{eff} SCSs are, respectively, called Affine, Secant, Tangent and m^{eff} models in the rest of the present paper.

3. Results and discussions

The material studied in the present paper is magnesium alloy AZ31B sheet, which has a hexagonal crystallographic structure with $c/a = 1.624$. The initial texture, shown in Fig. 1 as {00.2} and {10.0} pole figures, and the room temperature mechanical behavior of the sheet have been reported by Jain and Agnew (2007). Plastic deformation of AZ31B sheet is assumed to be due to Basal $\langle a\rangle$ ($\{00.1\}\langle 11.0\rangle$), Prismatic $\langle a\rangle$ ($\{10.0\}\langle 11.0\rangle$) and Pyramidal $\langle c+a\rangle$ ($\{11.2\}\langle 11.3\rangle$) slip systems, and $\{10.2\}\langle 10.1\rangle$ tensile twin system (Fig. 2). In all the numerical simulations reported in the present paper, uniaxial tension/compression is characterized by imposing the strain rate in the loading direction, while the only non-zero stress component is the normal stress along the loading direction. Thus, in addition to the normal strains in the width and thickness direc-

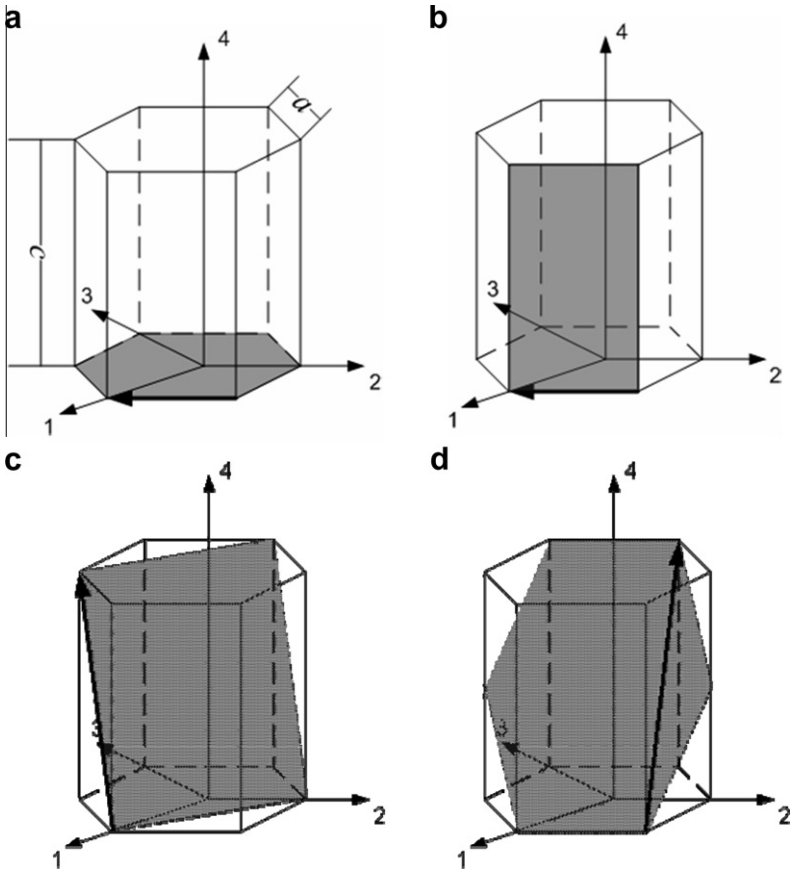

Fig. 2. Plastic deformation modes in hexagonal structure: (a) Basal $\langle a\rangle$ slip systems, (b) prismatic $\langle a\rangle$ slip systems, (c) pyramidal $\langle c+a\rangle$ slip systems, and (d) tensile twin.

Table 1
List of material constants for various self-consistent models.

Model	Mode	τ_0	τ_1	h_0	h_1	Latent	A^{th1}	A^{th2}
Affine	Basal	9	1	5000	25	4		
	Prismatic	79	40	590	50	4		
	Pyramidal	100	100	5000	0	2		
	Tensile twin	47	0	0	0	4	0.72	0
Secant	Basal	13	4	5000	30	4		
	Prismatic	73	35	400	60	4		
	Pyramidal	110	83	2500	0	2		
	Tensile twin	31	0	0	0	4	0.82	0
m^{eff} ($m^{eff} = 0.1$)	Basal	17	6	3800	100	4		
	Prismatic	77	33	650	50	4		
	Pyramidal	148	35	9600	0	2		
	Tensile twin	33	0	0	0	4	0.81	0
Tangent	Basal	21	5	3000	140	4		
	Prismatic	90	15	580		4		
	Pyramidal	145	30	9600	70	2		
	Tensile twin	38	0	0	0	4	0.81	0

tions, three shear strains are allowed to develop in uniaxial tension/compression. The true stress and true plastic strain curves are plotted in terms of their absolute values.

In the present paper, the reference slip/twinning rate $\dot{\gamma}_0$ and rate sensitivity m are assumed to be the same for all slip/twinning systems, and are taken as $\dot{\gamma}_0 = 0.001\ s^{-1}$ and $m = 0.05$, respectively. Values of the other material parameters in the Taylor and VPSC model with various SCSs are estimated by curve-fitting numerical simulations of uniaxial tension and compression along the RD to the corresponding experimental data. Although the fitting is done manually, using a systematic approach facilitates doing so. For example, during in-plane uniaxial tension of a sheet with strong basal texture, tensile twinning and pyramidal slip occur rarely. Thus, uniaxial tension along the RD allows us to independently fit the material parameters associated with the basal and prismatic slip systems. On the other hand, uniaxial compression along the RD is dominated by twinning at small strains, while at large strains pyramidal slip becomes very active. Therefore, the measured stress and strain curve under uniaxial compression along the RD at small and large strains allows us to, respectively, determine the material parameters associated with the tensile twinning and pyramidal slip. The determined values of the material constants are listed in Table 1. It is important to point out that the values of the material parameters for the Taylor and Secant models are found to be the same, and the predictions of these two models are almost the same for all the deformation processes studied in the present paper. An assessment of the predictive capability of the VPSC model with the Secant scheme also applies to the classic Taylor model. Consequently, the results obtained for the Secant approach will be identified with those given by the Taylor model and the latter will not be presented in the present paper.

Figs. 3 and 4 present the uniaxial tension and compression stress and strain curves along the RD, respectively. It is found that all the models employed can reasonably fit the experimental curves. Figs. 5 and 6 present relative activities of slip/twinning under uniaxial tension and compression along the RD, respectively. As expected, there is negligible twinning activity under uniaxial tension (Fig. 5), while twinning is very active at small strains in all the models under uniaxial compression (Fig. 6). All models predict that, under uniaxial tension along the RD, mostly Basal and Prismatic slip accommodate the plastic deformation. Little or no Pyramidal slip or tensile twinning activity is predicted by any model. Under uniaxial compression along the RD and at strains $|\varepsilon| < 0.04$, tensile twinning is very active, most grains reorient their c-axis along the RD, and the remaining plasticity is accommodated by Basal slip. When the tensile twining activity is dramatically reduced, at a strain $\varepsilon \approx -0.04$, the Basal slip activity significantly increases in Affine, the Tangent and $m^{eff} = 0.1$ models, while it

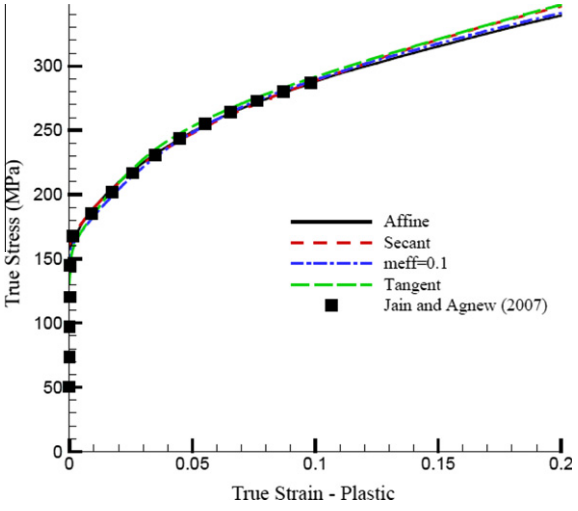

Fig. 3. Stress and strain curves under uniaxial tension along the RD.

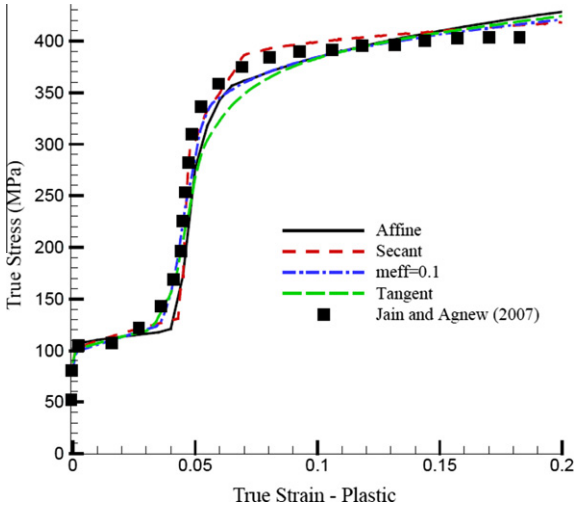

Fig. 4. Stress and strain curves under uniaxial compression along the RD.

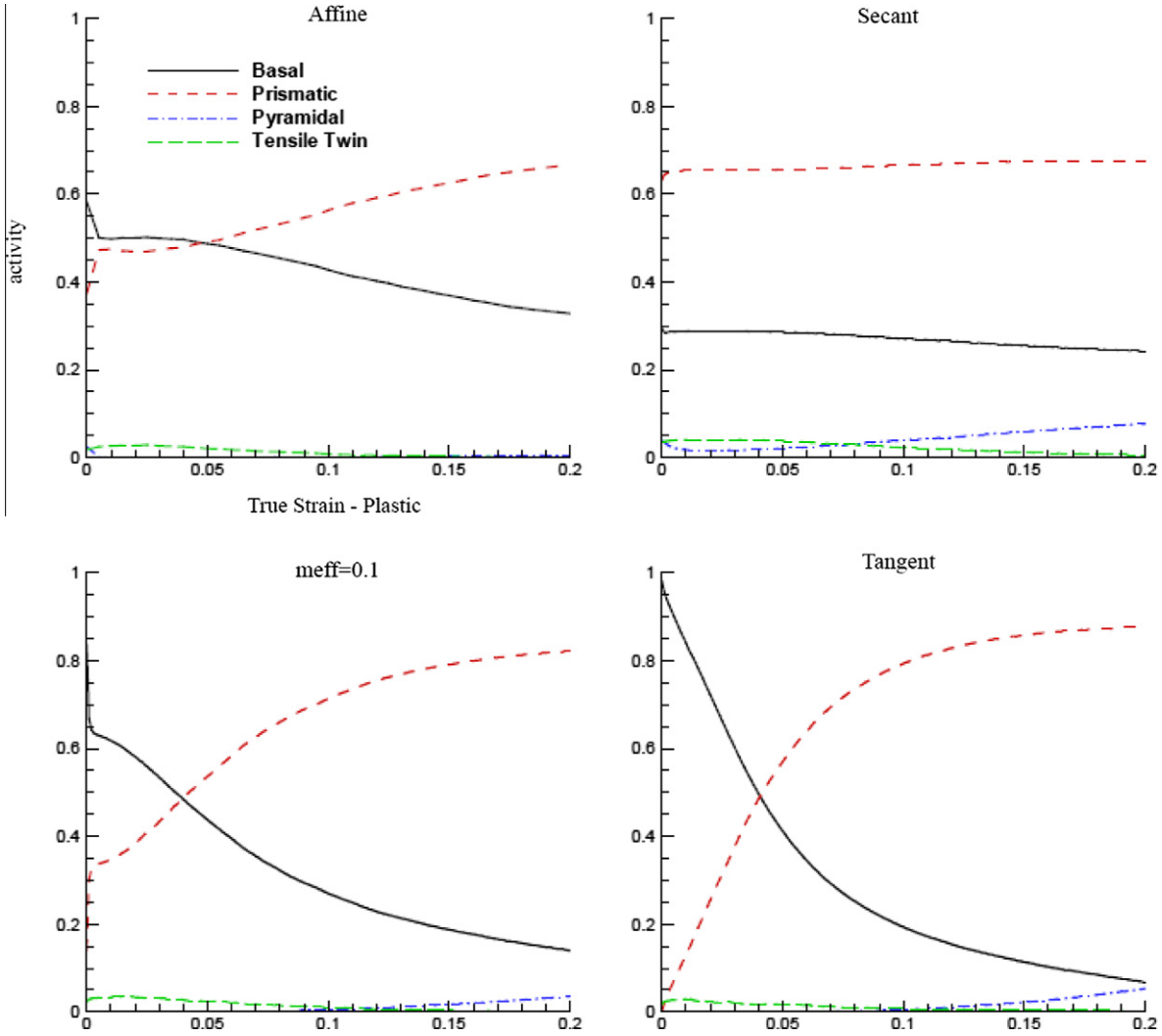

Fig. 5. Predicted slip/twinning activities for the sheet under uniaxial tension along the RD based on various polycrystal plasticity models.

slightly decreases in Secant model. For strains $|\varepsilon| > 0.04$ all the models predict increasing Pyramidal slip activity and little to no Prismatic slip. Both observations are a consequence of the previous twinning activity, which reorients the grains for tension along the *c*-axis. Fig. 7 shows the predicted deformation textures under uniaxial compression along the RD at strain $\varepsilon = -0.11$. Since, texture evolution is dominated by twinning reorientation, the deformation textures given by the various models are very close and are similar to the deformed texture measured experimentally (Jain and Agnew, 2007).

We proceed by numerically predicting the behavior of the sheet under uniaxial tension (Fig. 8) and compression (Fig. 9) along the TD, using the models and the corresponding values of material parameters determined above. It is clear that all the models numerically reproduce, with reasonable accuracy, the experimental stress and strain curves along the TD. Fig. 10 shows the predicted deformation textures under uniaxial compression along the TD at strain $\varepsilon = -0.11$. It is again found that the deformation textures predicted by the various models are all similar to the measured textures (Jain and Agnew, 2007).

Fig. 11 presents the predicted and measured stress and strain curves under uniaxial compression along the ND. This comparison is an independent test of the model parameters. It is found that the Affine and Secant models give close agreement with the experimental curve at strains $|\varepsilon| < 0.05$. At large strains, the Affine shows a non-zero hardening rate and overestimates the flow stress. The Tangent and $m^{eff} = 0.1$ models remarkably underestimate the flow stress when $|\varepsilon| < 0.05$ and slightly overestimate the hardening at large strains. Although the stress and strain curves based on various models are quite different, the predicted textures, not shown here, are found to be very similar because twinning is not active and little texture evolution takes place at these strains. The differences in the predicted stress responses between various models (Fig. 11) result from the different slip activities in these models. Fig. 12 presents relative activities of slip/twinning under uniaxial compression along the ND. It is seen that the predicted activities in Prismatic slip and tensile twinning are low or zero for all the models throughout the deformation process. The Basal and Pyramidal activities, however, differ substantially from model to model: while Basal slip is the most important contributor (65–80%) in the Affine, Pyramidal slip dominates and contributes about 60% of the plastic deformation in the Secant. The predicted slip/twinning activities in the Tangent and $m^{eff} = 0.1$ models are quite similar, but different from Secant and Affine: Basal slip dominates when deformation is small and Pyramidal slip is the most active slip system at large strain. The prevalence of Basal slip at small strains results in the very low flow stresses predicted by the Tangent and $m^{eff} = 0.1$ models at small strains.

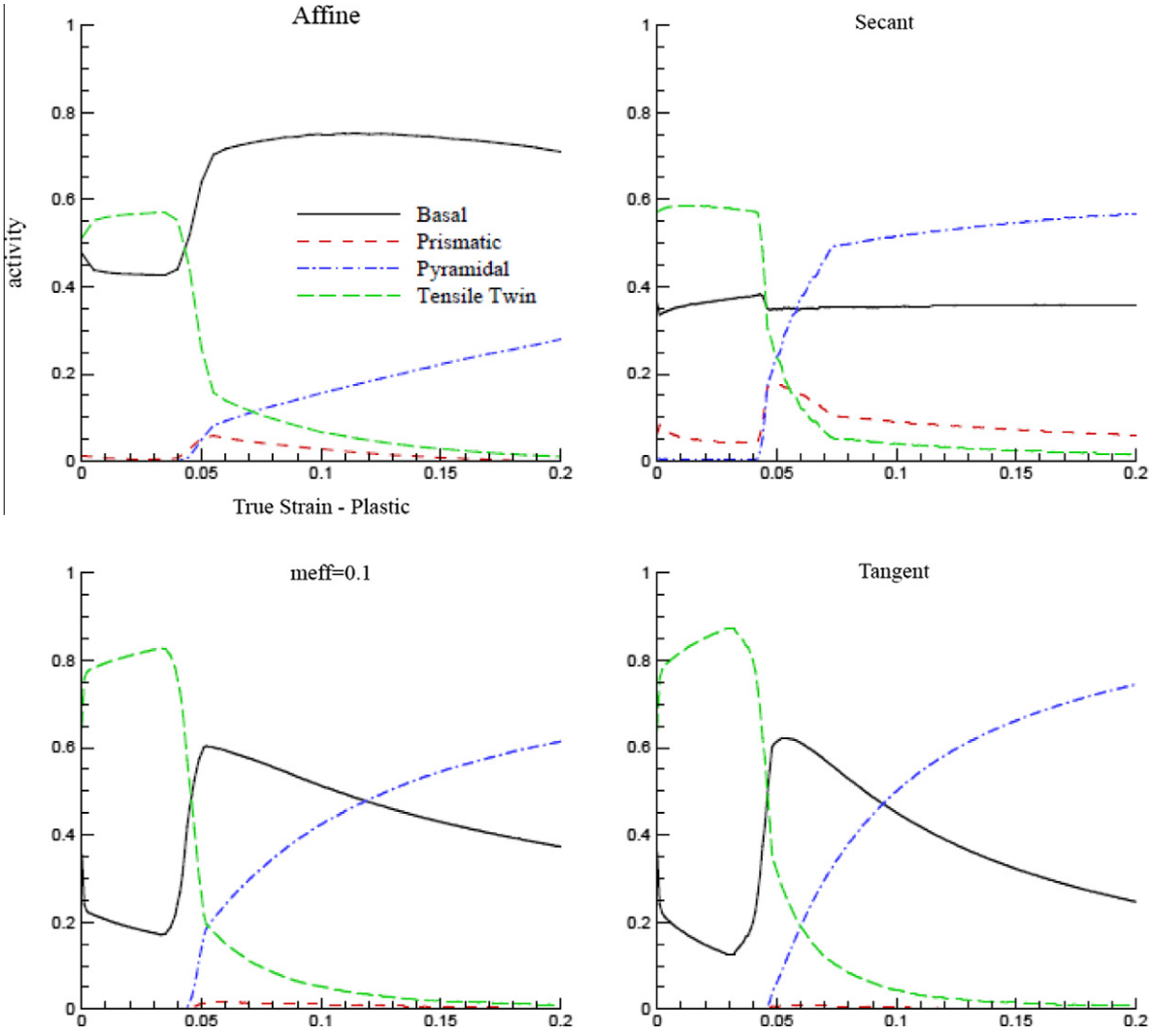

Fig. 6. Predicted slip/twinning activities for the sheet under uniaxial compression along the RD based on various polycrystal plasticity models.

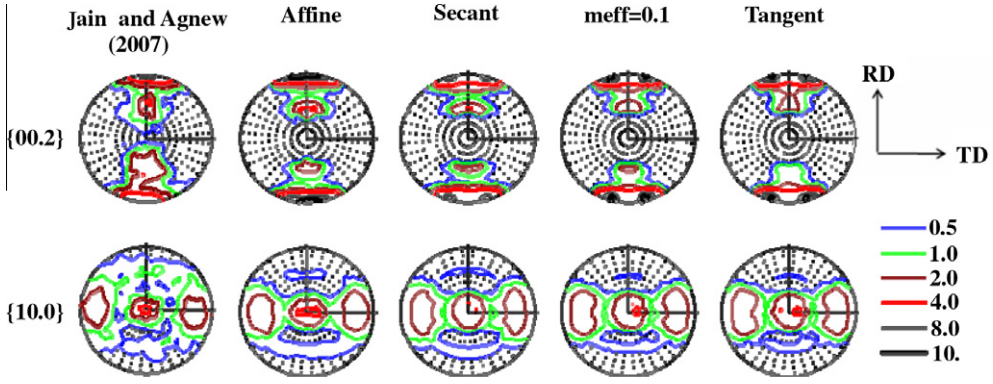

Fig. 7. Deformed textures under uniaxial compression along the RD at strain $\varepsilon = -0.11$.

In the sheet metal forming industry, the so-called R value, defined as transverse-to-thickness plastic strain-ratio under uniaxial tension within the sheet plane, is often used to characterize the anisotropy of the sheet. The measured R values are often used to calculate material parameters involved in anisotropic yield functions (see e.g. Wu et al., 2003; Barlat et al., 2006; Plunkett et al., 2008). Here, the prediction of R values will provide an independent test of the validity of each model. Fig. 13 shows the predicted and measured in-plane R value vs. angle with respect to the RD, for uniaxial tension at strain $\varepsilon = 0.11$. It is important to point out that the results in Fig. 13a and b are the same but plotted in different scales. It is observed that the Secant model (also the Taylor model) grossly overestimates the R values (Fig. 13a). The results based on the Affine and $m^{eff} = 0.1$ models are in good agreement with the experi-

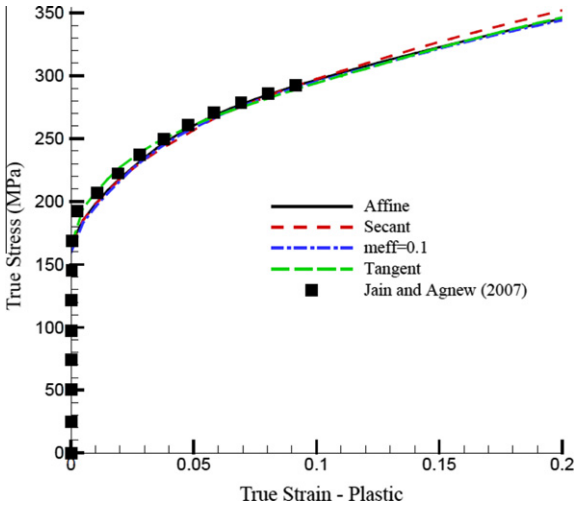

Fig. 8. Stress and strain curves under uniaxial tension along the TD.

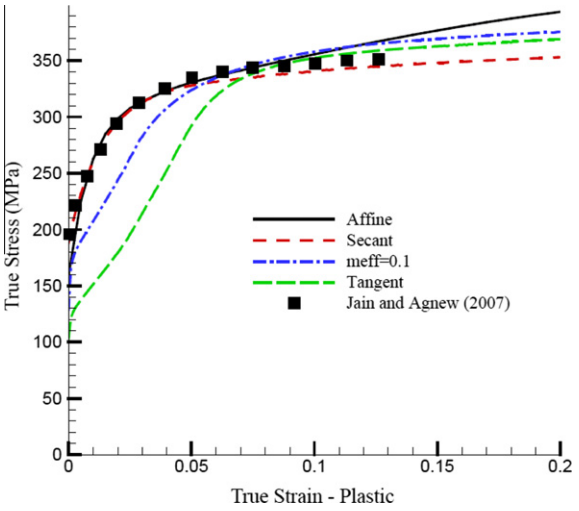

Fig. 11. Stress and strain curves under uniaxial compression along the ND.

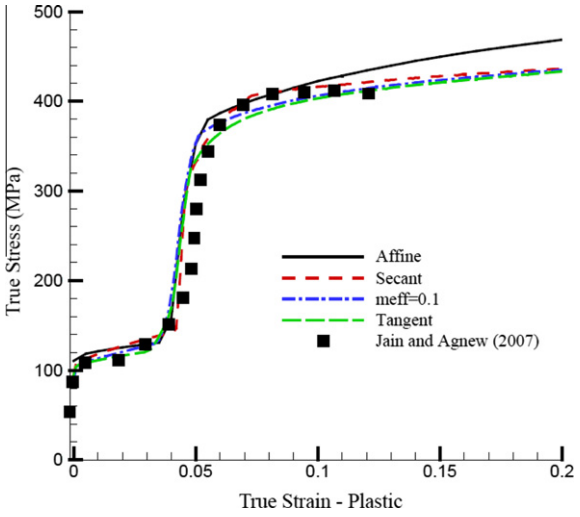

Fig. 9. Stress and strain curves under uniaxial compression along the TD.

mental data, while the Tangent model underestimates R slightly (Fig. 13b). As mentioned previously, the measured R values are often used to calculate material parameters involved in anisotropic yield functions. These anisotropic yield functions are such that R is often assumed to be constant with strain. This assumption, although not necessary, is reasonable in the yield functions designed for FCC and BCC polycrystalline sheets because variations in R values with applied deformation are relatively small (Barlat et al., 2006). However, for HCP materials, such as the magnesium alloy AZ31B sheet studied in the present paper, the predicted R value evolves significantly with straining, as shown in Fig. 14 for the sheet under uniaxial tension along the TD. It is very important to point out that the variation in R value with imposed tensile straining shown in Fig. 14 is confirmed by the experimental works on magnesium alloys at room temperature (Avery et al., 1965; Kaiser et al., 2003; Agnew and Duygulu, 2005; Hartig et al., 2005; Lou et al., 2007; Del Valle and Ruano, 2009). One may argue that significant change in R value with deformation is mainly due to texture evolution. However, even when texture evolution is excluded in the numerical simulations, the predicted R value still noticeably evolves with deformation, except in the simulation based on Affine model, where a constant R value ($R \approx 3.6$) is calculated. In short, Fig. 14 clearly indicates that the assumption of constant in-plane R value under uniaxial tension for determining material constants in anisotropic yield functions for HCP polycrystalline sheets is not appropriate. One may then ask a question: is it appropriate to use the in-plane R value under uniaxial compression for developing anisotropic yield functions for HCP polycrystalline sheets?

Fig. 15 plots the predicted R value vs. true plastic strain, based on the Affine model, under uniaxial compression along 0, 45° and 90° with respect to the RD. It is found that the predicted R value at small strains is negative. For isotropic materials and anisotropic FCC and BCC sheet metals under uniaxial compression, the width strain ε_w and thickness strain ε_t are both tensile. However, in the AZ31B sheet

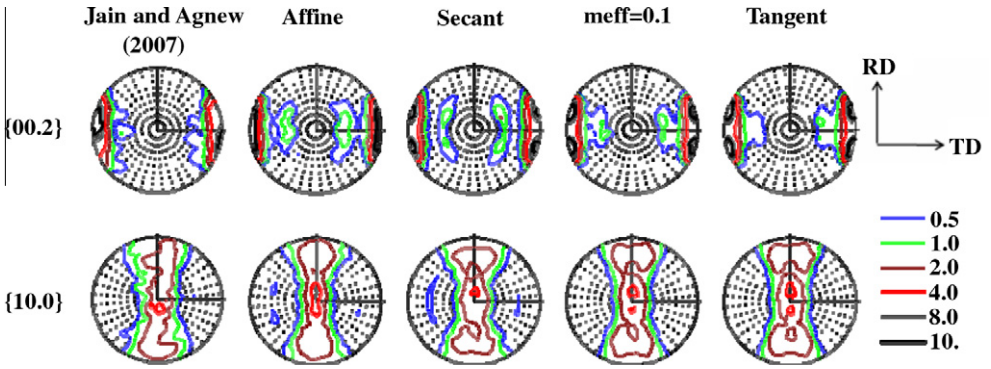

Fig. 10. Deformed textures under uniaxial compression along the TD at strain $\varepsilon = -0.11$.

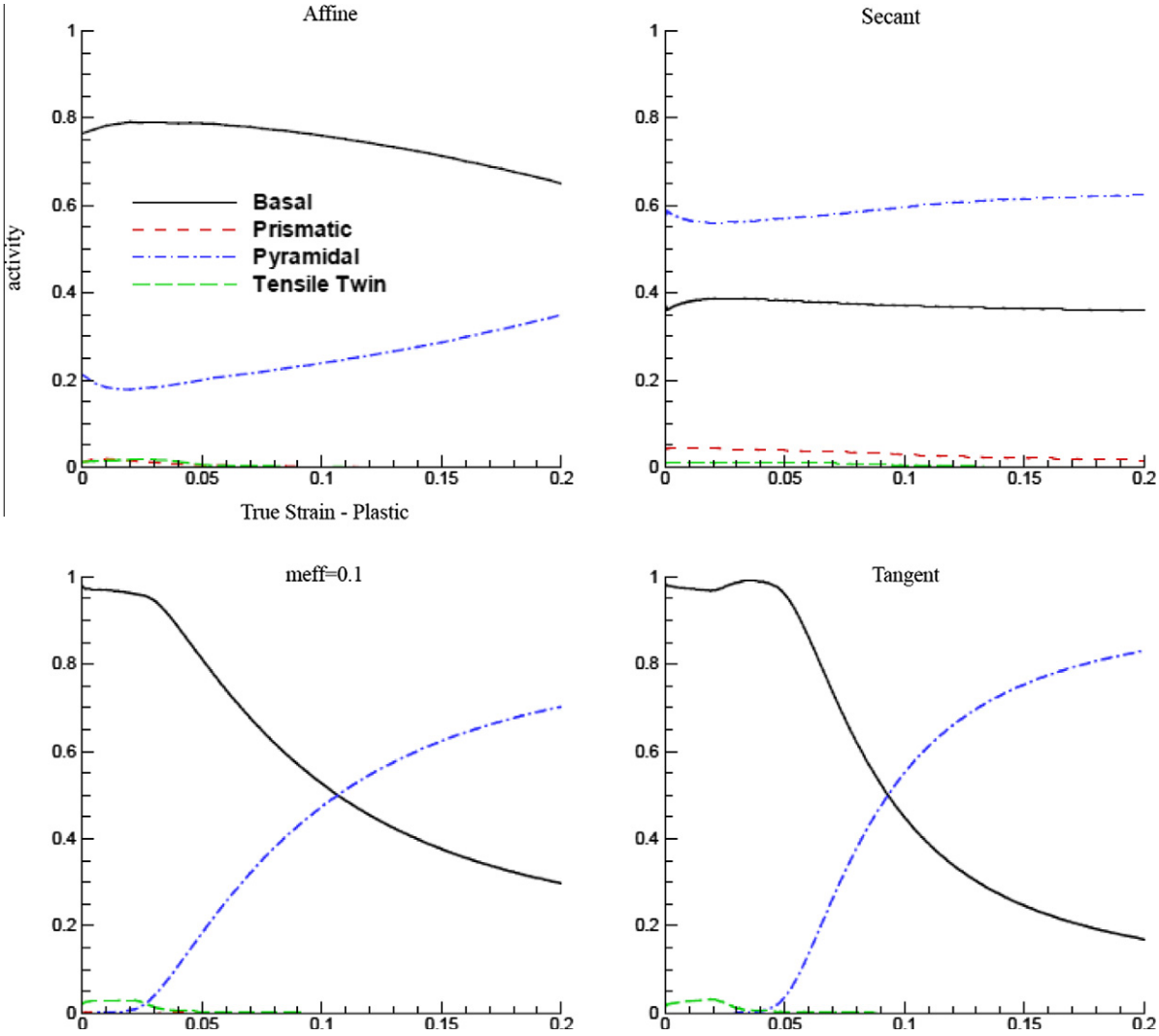

Fig. 12. Predicted slip/twinning activities for the sheet under uniaxial compression along the ND based on various polycrystal plasticity models.

under uniaxial compression, the Affine model predicts $\varepsilon_w < 0$ and $\varepsilon_t > 0$ at small strains when the tensile twinning occurs (see Fig. 10). At large strains, the predicted R value becomes positive because the width strain ε_w and thickness strain ε_t are both tensile. The other models predicted R value trends similar to those shown in Fig. 15. It should be pointed out that the predicted negative R value at small strains shown in Fig. 15 is not an artifact of the rigid, viscoplastic formulation of the VPSC model. The calculated R values predicted by the EVPSC model (when elasticity is accounted for) with the Affine self-consistent scheme are very close to the ones shown in Fig. 15 even at very small plastic strains. The predicted and measured R values under uniaxial compression within the sheet plane are presented in Fig. 16. It is seen that the $m^{eff} = 0.1$ and Tangent models give the best prediction, the Affine reasonably reproduces the experimental data, and the Secant model underestimates the experimental R value under uniaxial compression along the TD.

Under uniaxial compression along the ND, the R value is defined as the ratio of plastic strain in the RD to the plastic strain in the TD (Jain and Agnew, 2007). Fig. 17 shows the predicted R values based on the models and their comparison with the corresponding experimental R. It is found that the predicted R values are below, but relatively close to, the experimental R value. Detailed observation indicates that the Affine, $m^{eff} = 0.1$ and Tangent models give better agreement than the Secant.

We recall that Secant model predicts extremely high R values under uniaxial tension within the sheet plane (Fig. 13a and Fig. 14). Our numerical testing indicates that the predicted in-plane R value under uniaxial tension monotonically decreases with increasing CRSS ratio of Prismatic slip to Basal slip (see also Agnew and Duygulu, 2005), and monotonically increases with increasing CRSS ratio of Pyramidal slip to Prismatic slip. Based on these observations, we tried adjusting the values of the material parameters in Secant model to model the measured R values and the uniaxial tensile stress curve along RD. However, we found that there was no combination of parameters for which the Secant model could simultaneously predict reasonably the R values and measured stress–strain curves along the TD and ND. We also recall that the Tangent and $m^{eff} = 0.1$ models significantly underestimate the measured flow stress at small strains under uniaxial compression along ND (Fig. 11). We adjusted the material parameters in these models and found that, while the prediction of uniaxial compression along ND was truly improved, the predictions of other strain paths worsened. It seems that values of the material parameters, determined by fitting uniaxial tension and compression stress curves along the RD and listed in Table 1, give the best overall performance for each individual model.

Based on the numerical results, it can be concluded that among the examined models, those with interaction stiffness halfway be-

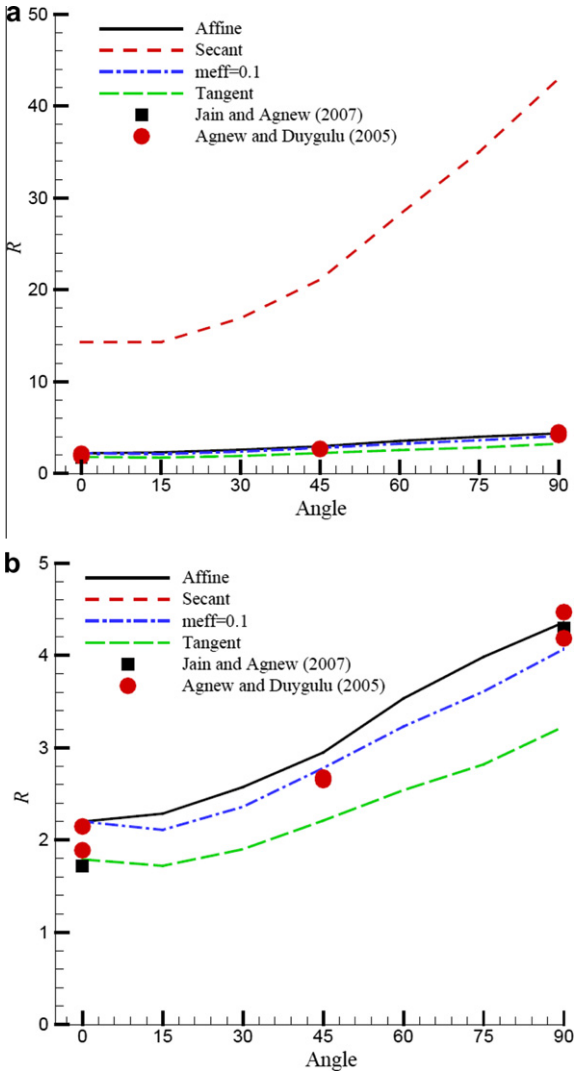

Fig. 13. *R* values under uniaxial tension within the sheet plane. Same results are plotted in different scales in (a) and (b).

tween the Secant (stiff) and Tangent (compliant) give the best results. In particular, no model gives a better overall performance than the Affine self-consistent. The fact that the Affine gives a good overall performance is a promising indication, because the Affine model requires no artificial "tuning" like the m^{eff}, but is based on a formal Tangent linearization of the response of grains and medium, as opposed to making the Tangent modulus proportional to the Secant modulus as suggested by Hutchinson (1976).

The advantage of the Affine scheme over the m^{eff} is further demonstrated in Fig. 18. In this figure, the dependence of the critical resolved shear stress (CRSS) ratios of non-Basal, namely Prismatic slip and Pyramidal slip to Basal slip are depicted for different m^{eff} values. The grain–matrix interaction stiffness (see Eq. (15)) is adjusted within the range $m^{eff} = 0.002 - 0.5$, which includes the compliant Tangent approximation $m^{eff} = 0.05$ and approaches the stiff Secant approximation, $m^{eff} = 1$. For this final aspect of the study, the slip system hardening parameters which give the best overall fits to the slip-dominated cases (uniaxial tension along RD and TD and uniaxial compression along ND) are determined. The cases involving significant twinning (e.g., in-plane compression) were avoided in order to simply characterize the impact of grain interaction stiffness on the slip system fit parameters. As the m^{eff} scheme is tuned to a stiffer grain–matrix interaction, i.e. as the m^{eff} value goes up, the non-Basal to Basal CRSS ratios necessary to obtain a good fit to the experimental results also increases. Interestingly, the best overall fits to the experimental data were obtained for the m^{eff} scheme when $0.1 < m^{eff} \leqslant 0.2$, and the CRSS ratios obtained within this range of m^{eff} values are very similar to those obtained via the Affine scheme.

Finally, we would like to underscore the previously observed fact that the relative strengths of slip systems determined from polycrystal simulations of magnesium alloys have been found to be at odds with historical single crystal magnesium results (see e.g. Koike and Ohyama, 2005). As an example, the non-basal to basal CRSS ratios obtained in the present study for the initial CRSS's associated with the Affine linearization schemes are in the range of 8–12. This range of ratios is higher than those of many recently published reports, which emphasizes the importance of the interaction stiffness in such studies. Nevertheless, it is still much lower than those empirically measured on pure Mg single crystals (Sheerly and Nash, 1960; Yoshinaga and Horiuchi, 1963; Akhtar and Teghtsoonian, 1969a,b; Obara et al., 1973). We attribute such difference to the fact that a single crystal deforms mainly by single slip, dislocations have to overcome only the Peierls stress, and they can exit through the free surface of the crystal. For a grain within the bulk of an aggregate, on the other hand, dislocations are arrested at grain boundaries, which induce reaction stresses, cross slip, a rapid increase of the dislocation population and a rapid hardening rate.

4. Conclusions

In this paper, various self-consistent polycrystal plasticity models have been evaluated by studying large strain behavior of magnesium alloy AZ31B sheet under different deformation processes. In all the polycrystal plasticity models considered, both slip and twinning contribute to plastic deformations. The material parameters for the various models were first fitted to experimental uniaxial tension and compression curves along the RD and then used to predict uniaxial tension and compression along the TD and uniaxial compression in the ND. An assessment of the predictive capability of the polycrystal plasticity models has been made based on comparisons of the predicted and experimental stress responses and *R* values. It is interesting to point out that the estimated values of the material parameters for the classical Taylor and Secant models were found to be the same, and the predictions of these two models were almost the same for all the deformation processes studied in the present paper. An assessment of the predictive capability of the VPSC model with the Secant scheme also applied to the classic Taylor model. It has been demonstrated that, among the models examined, the VPSC model with the Affine self-consistent model gives the best overall performance and requires no artificial tuning as does the m^{eff} scheme.

Our numerical results have clearly indicated that the *R* values under uniaxial tension and compression within the sheet plane evolve remarkably with imposed strain. This suggests that using *R* values measured at a given strain to determine anisotropic constants in anisotropic yield functions for HCP polycrystals is not appropriate for other strains.

It is important to point out that the main purpose of the present paper is to evaluate various homogenization assumptions for predicting the mechanical behavior of polycrystalline materials from the responses of their single crystals, while the basic descriptions of plastic deformation of the single crystals are the same for all the models. More specifically, the slip/twining hardening is described by (6) and (7) and twinning is characterized by the PTR model. The evaluation made in the present paper depends on the single crystal plasticity linearization employed. More advanced slip and twinning models have been developed (see e.g. Kalidindi,

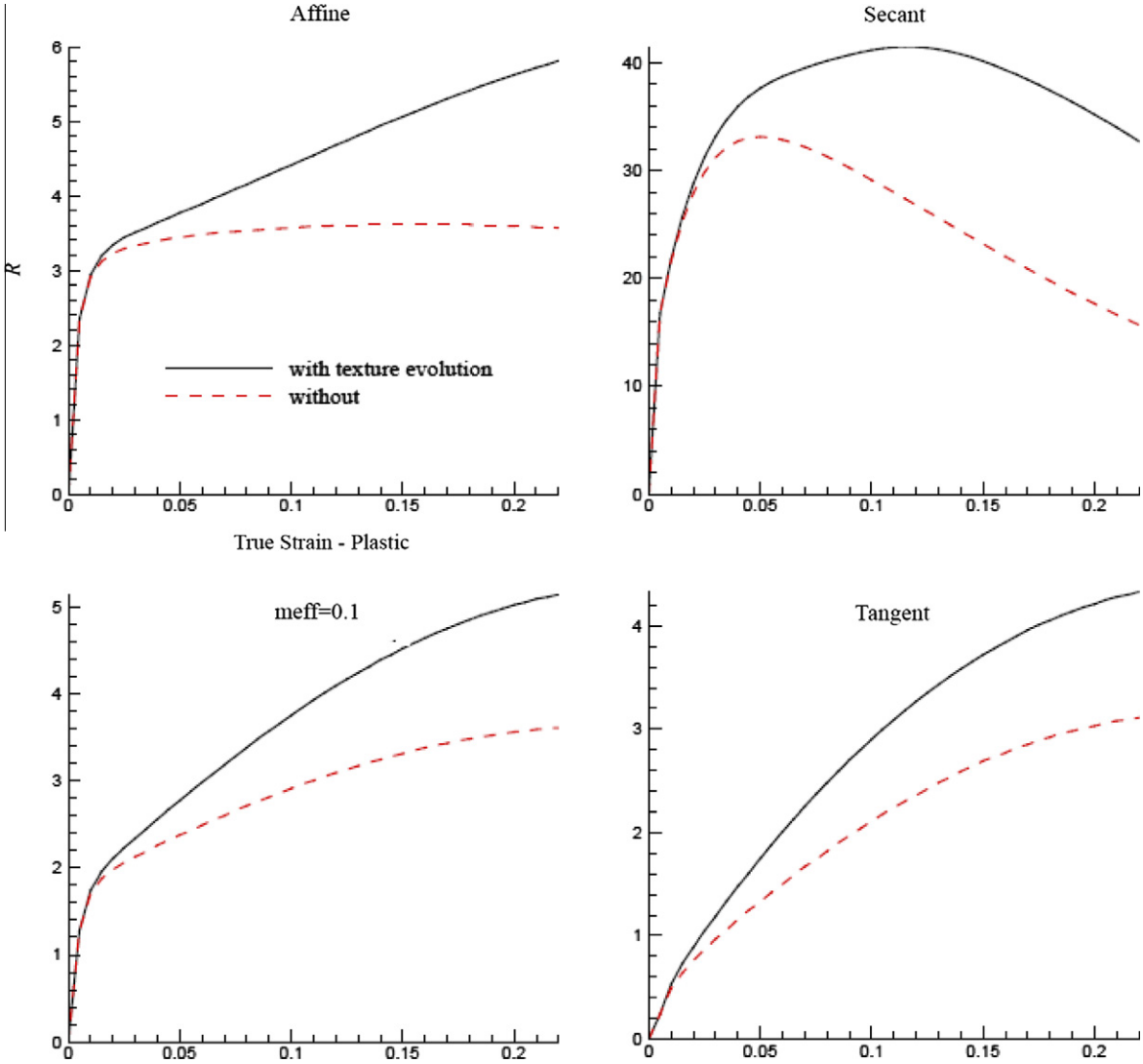

Fig. 14. Predicted *R* value vs. true plastic strain curves under uniaxial tension within the sheet plane based on various polycrystal plasticity models.

1998, 2001; Staroselsky and Anand, 2003; Wu et al., 2007a; Beyerlein and Tomé, 2008; Proust et al., 2009). An assessment of the validity of the various homogenization methods by comparison with local field calculations done by Fast Fourier Transform technique have been reported by Lebensohn et al. (2007). The authors conclude that a linearization based on accounting for (first order)

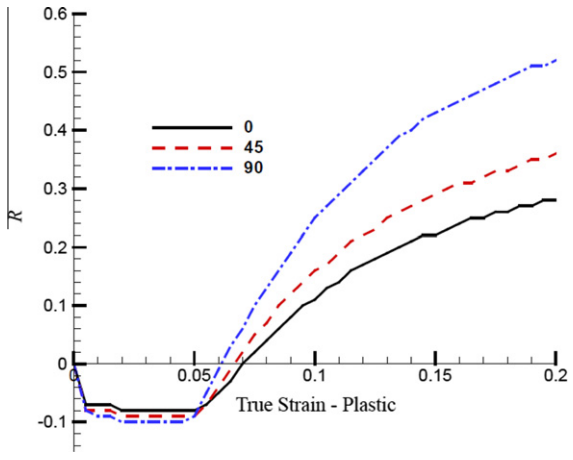

Fig. 15. Predicted *R* value vs. true plastic strain curves under uniaxial compression within the sheet plane based on Affine model.

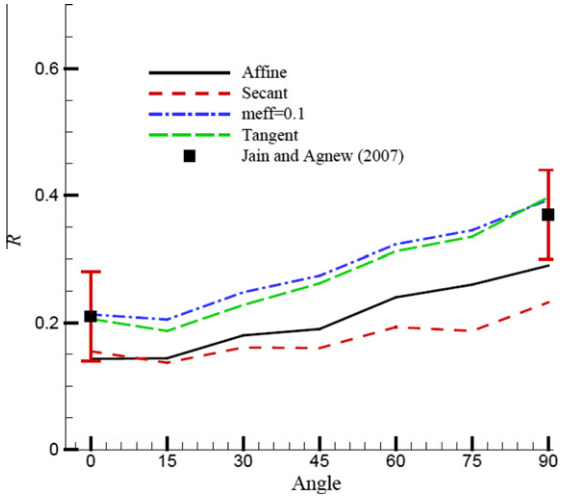

Fig. 16. *R* values under uniaxial compression within the sheet plane.

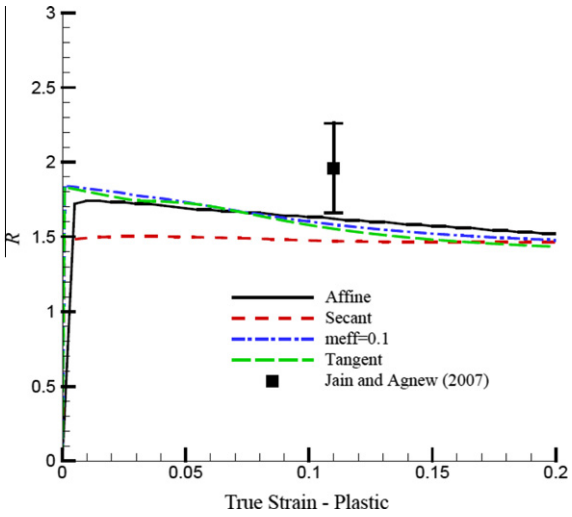

Fig. 17. *R* values under uniaxial compression along the ND.

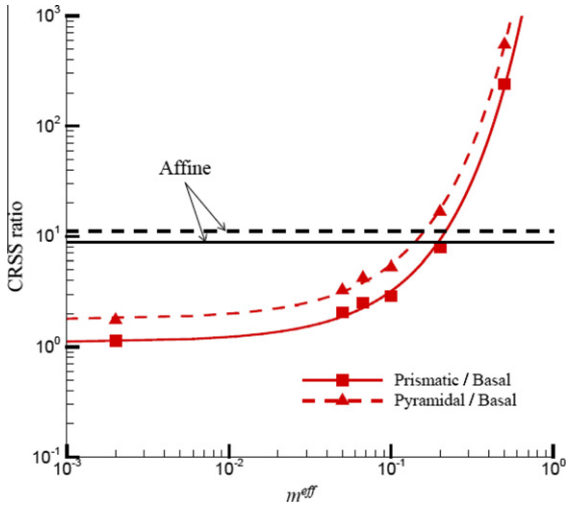

Fig. 18. Dependence of the fitted critical resolved shear stress (CRSS) ratios of Prismatic and Pyramidal slips to Basal slip on the grain interaction stiffness (different m^{eff} values). CRSS values determined from fits to experimental stress–strain curves and *R* values of slip-dominated strain paths. Corresponding ratios for Affine self-consistent scheme also depicted.

stress fluctuations inside the grains provides a good match with the results of a full-field calculation, especially when the plastic anisotropy of the grains is large (see Fig. 2 in Lebensohn et al. (2007)).

It is important to mention that self-consistent polycrystal plasticity models consider the interaction between a given grain and a "homogenized matrix" representing the rest of the materials, but they do not take into account the specific interaction between an individual grain and its neighboring grains. When the phenomenon to be studied depends on the local characteristics and heterogeneity of such interaction (stress–strain response, Lankford coefficient and texture evolution are not particularly sensitive to local effects), then Crystal Plasticity Finite Element Models (CPFEM) may be required. In CPFEM simulations, an element of the finite element mesh represents either a single crystal or a part of a single crystal, and the constitutive response at an integration point is described by the single crystal constitutive model. This approach enforces both equilibrium and compatibility throughout the polycrystalline aggregate in the weak finite element sense (see e.g. Anand and Kalidindi, 1994; Wu et al., 2004). Furthermore, this approach facilitates taking into account grain morphology and modeling of inhomogeneous deformations at the crystal level (Wu et al., 2006, 2007b; Shi et al., 2010).

Acknowledgements

This research was supported by funding from the NSERC Magnesium Strategic Research Network. More information on the Network can be found at www.MagNET.ubc.ca. CT and SA acknowledge support from Office of Basic Energy Sciences (DOE), Project FWP 06SCPE401. Dr. A. Jain is gratefully acknowledged for help with the texture analysis. BR is grateful for the support of the United States Automotive Materials Partnership (USAMP) which is, in turn, funded by the US Department of Energy National Energy Technology Laboratory under Award Number DE-FC26-02OR22910.

References

Agnew, S.R., Duygulu, O., 2005. Plastic anisotropy and the role of non-basal slip in magnesium alloy AZ31B. Int. J. Plast. 21, 1161–1193.
Akhtar, A., Teghtsoonian, E., 1969a. Solid solution strengthening of magnesium single crystals-I. Alloying behaviour in basal slip. Acta Metall. 17, 1339–1349.
Akhtar, A., Teghtsoonian, E., 1969b. Solid solution strengthening of magnesium single crystals-II. The effect of solute on the ease of prismatic slip. Acta Metall. 17, 1351–1356.
Anand, L., Kalidindi, S.R., 1994. The process of shear band formation in plane strain compression of FCC metals: effects of crystallographic texture. Mech. Mater. 17, 223–243.
Asaro, R.J., Needleman, A., 1985. Texture development and strain hardening in rate dependent polycrystals. Acta Metall. Mater. 33, 923–953.
Avery, D.H., Hosford, W.F., Backofen, W.A., 1965. Plastic anisotropy in magnesium alloy sheets. Trans. Metall. Soc. AIME 233, 71–78.
Barlat, F., Yoon, J.W., Cazacu, O., 2006. On linear transformation based anisotropic yield functions. Int. J. Plast. 23, 876–896.
Beyerlein, I.J., Tomé, C.N., 2008. A dislocation based constitutive law for pure Zr including temperature effects. Int. J. Plast. 24, 867–895.
Dawson, P.R., MacEwen, S.R., Wu, P.D., 2003. Advances in sheet metal forming analyses: dealing with mechanical anisotropy from crystallographic texture. Int. Mater. Rev. 48, 86–122.
Del Valle, J.A., Ruano, O.A., 2009. Effect of annealing treatments on the anisotropy of a magnesium alloy sheet processed by severe rolling. Mate. Lett. 63, 1551–1554.
Eshelby, J.D., 1957. The determination of the elastic field of an ellipsoidal inclusion, and related problems. Proc. Royal Soc. Lond. A241, 376–396.
Eyckens, P., Van Bael, A., Van Houtte, P., 2009. Marciniak–Kuczynski type modelling of the effect of through-thickness Shear on the forming limits of sheet metal. Int. J. Plast. 25, 2249–2268.
Hartig, Ch., Styczynski, A., Kaiser, F., Letzig, D., 2005. Plastic anisotropy and texture evolution of rolled AZ31 magnesium alloys. Mater. Sci. Forum, 1615–1620.
Hill, R., 1965. Continuum micro-mechanics of elastoplastic polycrystals. J. Mech. Phys. Solids 13, 89–101.
Hutchinson, J.W., 1976. Bounds and self-consistent estimates for creep of polycrystalline materials. Proc. Royal Soc. Lond. A348, 101–127.
Jain, A., Agnew, S.R., 2007. Modeling the temperature dependent effect of twinning on the behavior of magnesium alloy AZ31B sheet. Mater. Sci. Eng. A462, 29–36.
Kaiser, F., Letzig, D., Bohlen, J., Styczynski, A., Hartig, Ch., Kainer, K.U., 2003. Anisotropic properties of magnesium sheet AZ31. Mater. Sci. Forum, 315–320.
Kalidindi, S.R., 1998. Incorporation of deformation twinning in crystal plasticity models. J. Mech. Phys. Solids 46, 267–290.
Kalidindi, S.R., 2001. Modeling anisotropic strain hardening and deformation textures in low stacking fault energy FCC metals. Int. J. Plast. 17, 837–860.
Koike, J., Ohyama, R., 2005. Geometrical criterion for the activation of prismatic slip in AZ61 Mg alloy sheets deformed at room temperature. Acta Mater. 53, 1963–1972.
Kröner, E., 1958. Berechnug der elastischen konstanten des vielkristalls aus den konstanten des einnkristalls. Zeitschrift Fur Phys. 151, 504–518.
Lebensohn, R.A., Tomé, C.N., 1993. A self-consistent anisotropic approach for the simulation of plastic deformation and texture development of polycrystals – application to zirconium alloys. Acta Metall. Mater. 41, 2611–2624.
Lebensohn, R.A., Tomé, C.N., 1994. A self-consistent viscoplastic model – prediction of rolling textures of anisotropic polycrystals. Mater. Sci. Eng. A175, 71–82.
Lebensohn, R.A., Tomé, C.N., Ponte Castañeda, P., 2007. Self-consistent modeling of the mechanical behavior of viscoplastic polycrystals incorporating intragranular field fluctuations. Phil. Mag. 87, 4287–4322.
Lebensohn, R.A., Turner, P.A., Signorelli, J.W., Canova, G.R., Tomé, C.N., 1998. Calculation of intergranular stresses based on a large strain visco-plastic self-consistent model. Model. Simul. Mater. Sci. Eng. 6, 447–465.
Lévesque, J., Inal, K., Neale, K.W., Mishra, R.K., 2010. Numerical modeling of formability of extruded magnesium alloy tubes. Int. J. Plast. 26, 65–83.

Lou, X.Y., Li, M., Boger, R.K., Agnew, S.R., Wagoner, R.H., 2007. Hardening evolution of AZ31B Mg sheet. Int. J. Plast. 23, 44–86.
Molinari, A., Canova, G.R., Ahzi, S., 1987. A self-consistent approach of the large deformation polycrystal viscoplasticity. Acta Metall. 35, 2983–2994.
Molinari, A., Tóth, L.S., 1994. Tuning a self-consistent viscoplastic model by finite element results. Part I: Modeling. Acta Metall. Mater. 42, 2453–2458.
Neil, C.J., Agnew, S.R., 2009. Crystal plasticity-based forming limit prediction for non-cubic metals: application to Mg alloy AZ31B. Int. J. Plast. 25, 379–398.
Obara, T., Yoshinaga, H., Morozumi, S., 1973. {11–22}⟨-1-123⟩ slip system in magnesium. Acta Metall. 21, 845–853.
Plunkett, B., Cazacu, O., Barlat, F., 2008. Orthotropic yield criteria for description of the anisotropy in tension and compression of sheet metals. Int. J. Plast. 24, 847–866.
Proust, G., Tomé, C.N., Jain, A., Agnew, S.R., 2009. Modeling the effect of twinning and detwinning during strain-path changes of magnesium alloy AZ31. Int. J. Plast. 25, 861–880.
Sheerly, W.F., Nash, R.R., 1960. Mechanical properties of magnesium monocrystals. Trans. Metall. Soc. AIME 218, 416–423.
Shi, Y., Wu, P.D., Lloyd, D.J., Embury, J.D., 2010. Crystal plasticity based analysis of localized necking in aluminum tube under internal pressure. Eur. J. Mech. A/Solids 29, 475–483.
Signorelli, J.W., Bertinetti, M.A., Turner, P.A., 2009. Predictions of forming limit diagrams using a rate-dependent polycrystal self-consistent plasticity model. Int. J. Plast. 25, 1–25.
Staroselsky, A., Anand, L., 2003. A constitutive model for HCP materials deforming by slip and twinning: application to magnesium alloy AZ31B. Int. J. Plast. 19, 1853–1864.
Taylor, G.I., 1938. Plastic strain in metals. J. Inst. Metals 62, 307–324.
Tomé, C.N., 1999. Self-consistent polycrystal models: a directional compliance criterion to describe grain interactions. Model. Simul. Mater. Sci. Eng. 7, 723–738.
Tomé, C.N., Lebensohn, R.A., Kocks, U.F., 1991. A model for texture development dominated by deformation twinning – application to zirconium alloys. Acta Metall. Mater. 39, 2667–2680.
Wang, H., Wu, P.D., Tomé, C.N., Huang, Y., 2010. A finite strain elastic–viscoplastic self-consistent model for polycrystalline materials. J. Mech. Phys. Solids 58, 594–612.
Wu, P.D., Huang, Y., Lloyd, D.J., 2006. Studying grain fragmentation in ECAE by simulating simple shear. Scripta Mater. 54, 2107–2112.
Wu, P.D., Jain, M., Savoie, J., MacEwen, S.R., Tugcu, P., Neale, K.W., 2003. Evaluation of anisotropic yield functions for aluminum sheets. Int. J. Plast. 19, 121–138.
Wu, X., Kalidindi, S.R., Necker, C., Salem, A.A., 2007a. Prediction of crystallographic texture evolution and anisotropic stress–strain curves during large plastic strains in high purity α-titanium using a Taylor-type crystal plasticity model. Acta Mater. 55, 423–432.
Wu, P.D., Lloyd, D.J., Jain, M., Neale, K.W., Huang, Y., 2007b. Effects of spatial grain orientation distribution and initial surface topography on sheet metal necking. Int. J. Plast. 23, 1084–1104.
Wu, P.D., MacEwen, S.R., Lloyd, D.J., Neale, K.W., 2004. A mesoscopic approach for predicting sheet metal formability. Model. Simul. Mater. Sci. Eng. 12, 511–527.
Wu, P.D., Neale, K.W., Van der Giessen, E., 1997. On crystal plasticity FLD analysis. Proc. Royal Soc. Lond. A453, 1831–1848.
Xu, F., Holt, R.A., Daymond, M.R., 2008. Modeling lattice strain evolution during uniaxial deformation of textured Zircaloy-2. Acta Mater. 56, 3672–3687.
Yoshinaga, H., Horiuchi, R., 1963. On the nonbasal slip in magnesium crystals. Trans. JIM 5, 14–21.